PROCEEDINGS, Thirty-Second Workshop on Geothermal Reservoir Engineering
Stanford University, Stanford, California, January 22-24, 2007
SGP-TR-183

CONVECTIVE DISPERSION IN A REAL FRACTURE

F. Bauget and M. Fourar

Ecole Nationale Supérieure des Mines de Nancy – LEMTA, Parc de Saurupt, 54042 Nancy Cedex France
e-mail: fabrice.bauget@ensem.inpl-nancy.fr
e-mail: mostafa.fourar@ensem.inpl-nancy.fr

ABSTRACT

Solute transport in fractured rocks is of major interest in many applications: geothermal energy production, petroleum industry, ground water management. This work focuses on a dispersion experiment performed with a transparent replica of a real fracture. The local aperture map was extracted using the well-known Beer-Lambert law, which shows a very heterogeneous medium. The hydrodynamic aperture was determined from single-phase flow measurements by assuming the validity of cubic law. Numerical simulation on the aperture map leads to the same aperture value. A tracer experiment was then performed at a Peclet number high enough to neglect molecular diffusion. While the classical convection-diffusion approach fails to interpret experimental results, a basic model of parallel rectangular ducts with local piston-like flow captures most of the breakthrough curve shape. The later corresponds to pure convection dispersion due to apertures and streamlines geometry distribution.

INTRODUCTION

Tracer flow in fractured rock is of great interest either in groundwater pollution, CO2 sequestration and oil recovery. This paper focuses on non-reactive solute transport in a single fracture with non-permeable walls. Solute transport is controlled by molecular diffusion and advection. In complex media, as real fracture and porous media, the heterogeneities also contribute to the dispersion of the solute at the macro-scale. Following previous works (Bodin et al. 2003a, Detwiler et al 2000) hydrodynamic dispersion in fracture may be divided into three processes which may be added: Taylor-Aris dispersion, roughness dispersion and aperture-variation dispersion. The first one occurs even with smooth walls due to the combined action of convection and radial molecular diffusion (Bear 1988, Dullien 1992). Equations in the following are written in one dimension with x the abscissa along the flow direction. The variables like velocity, concentration and flux, are averages done for each x over the cross section of the fracture. The mass balance equation is:

$$\phi \frac{\partial C}{\partial t} + \frac{\partial F}{\partial x} = 0 \qquad (1)$$

where C is the average solute concentration and F is the mass flux per unit area. ϕ is the porosity defined for the fracture as the ratio between the apertures average and the maximum aperture: $< h > / h_{\max}$ .In a piston-like displacement, the relation between the flux and the concentration is $F=UC$, with U the average velocity across the fracture. In a real fracture, heterogeneities at different scales, as rugosities and aperture variation, induce hydrodynamic dispersion. A common approach to model this process is based on a Fickian law giving the flux in accordance with the concentration and its gradient (Bear 1988, Dullien 1992):

$$F = UC - \phi D \frac{\partial C}{\partial x} \qquad (2)$$

which leads to the well-known advection-diffusion equation (Bear 1993):

$$\frac{\partial C}{\partial t} + \frac{U}{\phi} \frac{\partial C}{\partial x} = \frac{\partial}{\partial x}\left(D \frac{\partial C}{\partial x} \right) \qquad (3)$$

where D is the longitudinal hydrodynamic dispersion coefficient which depends on the three processes cited before. With smooth walls and a constant aperture, D is the Taylor-Aris dispersion coefficient (Dutta and Leighton 2001, Brenner and Edwards 1993): $D_m + f\left(U^2 h^2\right) / D_m$, where D_m is the molecular diffusion coefficient, h is the aperture and f is a constant depending on the cross section geometry. For a fracture with varying apertures, D has a similar form $D_m + \alpha U / \phi$ where α is the dispersivity (Bear 1993). For a homogeneous medium and for given initial and boundary conditions, analytical solutions of equation (3) may be easily derived. For example, with a step injection in a medium initially without solute:

$$\begin{cases} \text{if } \; t \le 0 \; \text{ then } \; c(x,t) = 0 \;\; \forall x \\ \text{if } \; t > 0 \; \text{ then } \; c(x,t) = C_0 \;\; \text{for } \; x = 0 \end{cases} \qquad (4)$$

the solution of equation (3) is (Bodin et al. 2003b):

$$\frac{C}{C_0}=\frac{1}{2}\left(\operatorname{erfc}\left(\frac{x-\frac{Ut}{\phi}}{2\sqrt{Dt}}\right)+e^{Ux/D\phi}\operatorname{erfc}\left(\frac{x+\frac{Ut}{\phi}}{2\sqrt{Dt}}\right)\right) \quad (5)$$

Two remarks may be done. First of all the catalyst of the dispersion process in the convection-diffusion approach (equation (3)) is the concentration gradient. Second this approach is extensively used even when molecular diffusion is negligible.

Another approach describing dispersion in fractured media is the channeling of the fluid flow (Bodin et al. 2003a, Neretnieks 2002, Grindrod and Impey 1993, Brown et al 1998). The process is controlled by preferential flow paths due to spatial variation of the aperture. The fracture may then be modeled by a distribution of channels along which particles are advected (Grindrod and Impey 1993, Neretnieks 2002). In other words, molecular diffusion is negligible and fluid particles displacement is only controlled by advection along streamtubes which are represented by channels.

This paper presents results of tracer dispersion experiment performed on a transparent replica of a real fracture. The image analysis is based on the Beer-Lambert law (Persoff and Pruess 1995, Isakov et al. 2001, Detwiler et al 2000, Lee et al. 2003). The first part presents the experimental setup and image analysis method. The experimental results are then detailed: single-phase flow measurements, apertures map determination and tracer experiment. Finally a discussion on experiment interpretation through different models shows that, neglecting molecular diffusion, advection allows to interpret and analyze the dispersion process observed when the classical convection-diffusion model fails.

EXPERIEMENTAL SETUP AND IMAGE PROCESSING

The resin replica of the fracture was made from a split block of Vosges sandstone. Its length is 330 mm (flow direction in the following), and its width is 148 mm. The details of the apertures measurements are presented in the results part. The replica is placed in a transparent acrylic glass holder allowing tracer and multiphase flow visualization. On one side four ports allow differential pressure measurements along the flow direction. The fluid injection was controlled either with a pharmacia pump (rate 5 $ml.h^{-1}$ to 499 $ml.h^{-1}$) or a Moineau pump allowing high flow rates up to 200 $l.h^{-1}$. Visualization was performed with a 2304x3456 resolution CCD camera leading to data of 1545x2760 after cropping over the fracture area. The light source was a Planistar light table giving homogeneous and constant lighting. A color filter is used in order to achieve the monochromatic source needed for the image processing described later. The solute is a blue copper-phthalocyanine dye and the particles size is in the range of 50 *nm* (Harris 1999). The molecular diffusion coefficient may be estimated using the Stokes-Einstein equation (Cussler 1984). A particle of 50 *nm* in water at 20 $^{\circ}C$ has a diffusion coefficient of 4.3×10^{-12} $m^2.s^{-1}$. A Taylor-Aris experiment in a rectangular duct gave 3.6×10^{-11} $m^2.s^{-1}$. The Peclet number defined by $Pe=(HU)/D_m$ is then greater than 5×10^3 with our experimental conditions: a flow rate of 100 $ml.h^{-1}$ and the measured hydraulic aperture H (Table (1)).

The intensity of a light going through a solution is attenuated according to the solute concentration and the solution thickness. The Beer-Lambert law gives the transmitted intensity I for a monochromatic incident light as follow (Detwiler et al 1999):

$$I = I_0\exp(-\varepsilon Ch) \quad (6)$$

where C is the solute concentration, h is the solution thickness and ε is the solute absorptivity. Attenuation due to the container is taken into account through I_0. Measuring the intensities and knowing the absorptivity, equation (6) allows the calculation of one of the two unknowns, h or C, from the knowledge of the other. Using a rectangular Plexiglas cell with a constant h = 5 *mm*, ε is first calculated by measuring the intensity for different concentrations. Figure (1) shows measurements done with concentrations varying from zero to C_0=0.85 $g.l^{-1}$ and equation (6). It gives $\varepsilon=1.12\pm0.07\times10^3$ $m^2.kg^{-1}$.

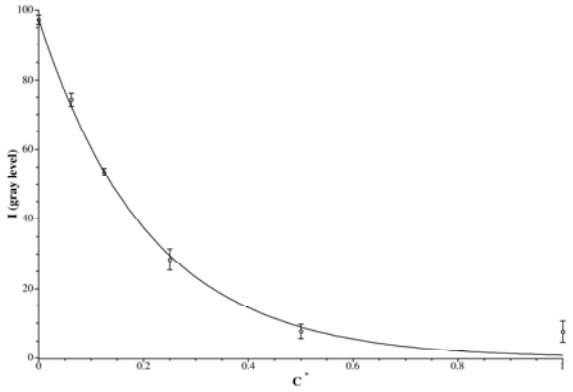

Figure 1: Solute absorptivity calibration: $C^*=C/C_0$, scatters are gray intensities, line is the Beer-Lambert law with ε = 1.12 ±0.07 $\times10^3$ $m^2.kg^{-1}$.

Considering the Beer-Lambert law valid at each pixel, two images are required to derive the apertures map over the entire fracture: one with the fracture filled with clear water (no solute) giving I_{0xy}, the second one with the void volume fully saturated with a solution at concentration C_0 giving I_{xy}. The

subscripts x and y are the pixels coordinates. The apertures map h_{xy} is then calculated with equation (6) (Figure (2)).

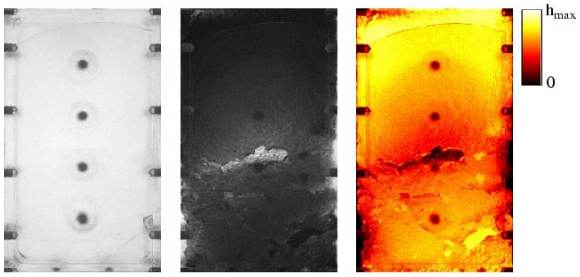

Figure 2: Apertures map determination: in image I_0 the fracture is saturated without solute, in image I it is saturated with a solution at C_0, h is the apertures map.

After which, from the knowledge of h_{xy}, I_{0xy} and ε, C_{xy} may be calculated during a tracer experiment by taking images at different time.

EXPERIEMENTAL RESULTS

Single-Phase Flow Experiments

A fracture is a complex object with different scales involved from rugosities to average aperture. The simplest hydraulic model of this object is a smooth fracture with a constant aperture H giving the same head loss. H is commonly called the hydraulic aperture. For a Poiseuille flow between two smooth planes with the width much greater than the aperture, the solution of the Navier-Stokes equation is well known (Zimmermann and Main 2004):

$$Q = \frac{wH^3}{12\mu}\frac{\Delta P}{L_x} \qquad (7)$$

where H is the aperture, μ is the fluid viscosity, ΔP is the pressure drop along the flow direction, w and L_x are respectively the width in the transverse direction and the length along the flow direction. By measuring the flow rate and the pressure gradient over the real fracture, we are able to derive the hydraulic aperture H. By analogy with the Darcy law for an incompressible fluid, the permeability would be $K = wh^3/(12A)$ with A the cross-sectional area. At high flow rate inertial effects lead to a deviation from the Darcy law as a non-linear relation (Fourar et al. 1993). Several empirical laws have been proposed (Bear 1988). The relationship most commonly used is the Forchheimer equation (Forchheimer 1914):

$$\frac{\Delta P}{L_x} = \frac{\mu}{K}\frac{Q}{A} + \beta\rho\frac{Q^2}{A^2} \qquad (8)$$

where ρ is the fluid density and β is the inertial coefficient. Using the analogy between Darcy law and Poiseuille flow in a smooth fracture, equation (8) may be rewritten in term of hydraulic aperture (Fourar et al. 1993):

$$\frac{\Delta P}{L_x} = \frac{12\mu}{H^3 w}Q + \frac{\beta\rho}{H^2 w^2}Q^2 \qquad (9)$$

In our experiment, we used water density and viscosity at standard conditions and w=148 mm. Three sets of experiments have been performed with a flow rate from 0 to 200 $l.h^{-1}$. Figure (3) shows equation (9) fitted to experimental data points. The least square method leads to H=413 μm and β = 44.6 m^{-1}.

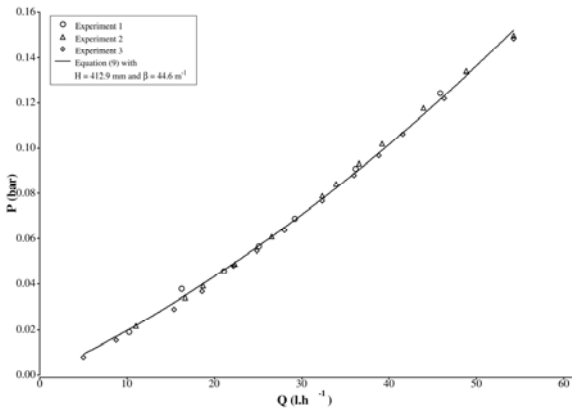

Figure 3: Monophasic experiments: scatters are experimental data sets, line is the Forchheimer equation plot with H = 413 μm and β = 44.6 m^{-1}.

Apertures Map Determination

Figure (1) shows that the Beer-Lambert law is valid for a product hC up to around 2.13 $g.m^{-2}$. Our goal here is to extract the aperture map over the entire fracture. Because h_{xy} is varying spatially up to a maximum h_{max}, we have to choose a concentration C_0 such as $C_0 h_{max} < 2.13\, g.m^{-2}$. Although the hydraulic conductivity is usually not equal to the arithmetic mean (Renard and de Marsily 1997), we may take the experimental value of H as an order of magnitude. This would give a maximum concentration around 5.16 $g.l^{-1}$. Considering that the maximum could be at least twice H, we chose C_0=2.55 $g.l^{-1}$.

As explained above an image of the fracture fully saturated with a solution at C_0 gives I at each pixel, a second one with clear water gives I_0. The apertures map is then easily obtained using equation (6) at each pixel. Figure (4) shows the aperture histogram. The main statistical characteristics are summarized in Table (1) with: h_a the arithmetic mean, h_h the harmonic mean, σ the standard deviation and V the

total volume. The harmonic mean has been calculated from the data set without the zero apertures that represent less than 1.1 % of the original 1545×2760 data (Figure (4)).

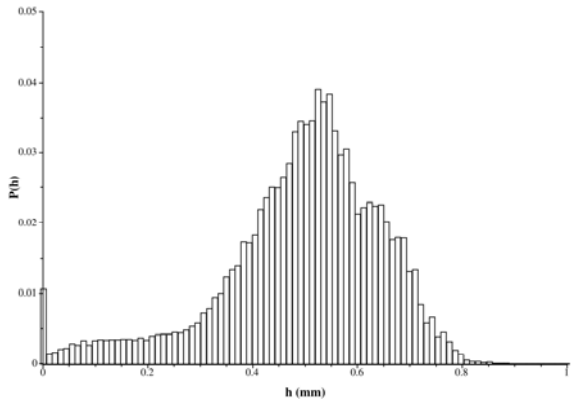

Figure 4: Normalized aperture histogram.

Figure (2) shows the extracted map with apertures ranging from 0 (black) to 1.091mm (white). The first half (bottom) is clearly more heterogeneous than the second. The dark area in the center corresponds to very small apertures which will strongly affect the dispersion process as it will be shown later. The averages h_a and h_h give good order of magnitudes with $h_a > H > h_h$ as it has often been observed (Renard and de Marsily 1997)). To further check the map extraction process validity from image analysis, hydraulic aperture is calculated numerically using this aperture field. The mesh is as each pixel is centered on an element volume $\delta y \delta x h_{xy}$ with δx the space step along the flow direction and δy in the transverse direction. Considering the fluid incompressible, $\nabla \cdot \mathbf{u} = 0$, equation (7) may be solved with $u_{xy} = Q/(\delta y h_{\max})$:

$$\nabla(\mathsf{K}\nabla P) = 0 \qquad (10)$$

where P is the local pressure and K is the spherical tensor of local conductivity with $h_{xy}^3/(12h_{max})$ as diagonal elements. Equation (10) is solved numerically using finite volume method. The boundary conditions are no-flow in the transverse direction and pressures are imposed at the inlet and the outlet. Calculation with no refinement gives H=447 μm which is in agreement with experimental value within 8.2 %. The map extraction is then validated with a reasonable error between the numerical and experimental hydraulic apertures.

Table 1: Apertures map characteristics

H (mm)	h_a (mm)	h_h (mm)	h_{max} (mm)	σ
0.448	0.497	0.363	1.091	0.156

Tracer Experiment

The tracer experiment was performed at a constant flow rate of 100 $ml.h^{-1}$. The concentration C_0 of the injected solution was 2.55 $g.l^{-1}$. Images were taken at intervals of time between 10 seconds and 180 seconds. Initial condition is $C=0$ over the entire fracture. The tracer is injected continuously at a constant rate (conditions (4)), and is supposed to be uniform over the inlet cross-sectional area. Figure (5) shows six images at different times. The effect of the small apertures area (see the apertures map determination section) is clearly observable with two main flow paths downstream which grow very slowly in the transverse direction.

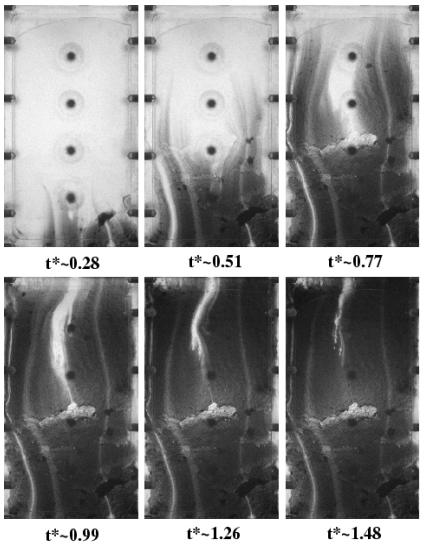

Figure 5: Tracer experiment: six images at different times $t^*=tQ/V$ with $Q=100$ $ml.h^{-1}$ and V the total volume (Table 1). Injection is from the bottom.

Figure (6) shows the average concentration versus time at four different positions along the flow direction x^*=0.25, x^*=0.5, x^*=0.75 and x^*=1, with $x^*=x/L_x$.

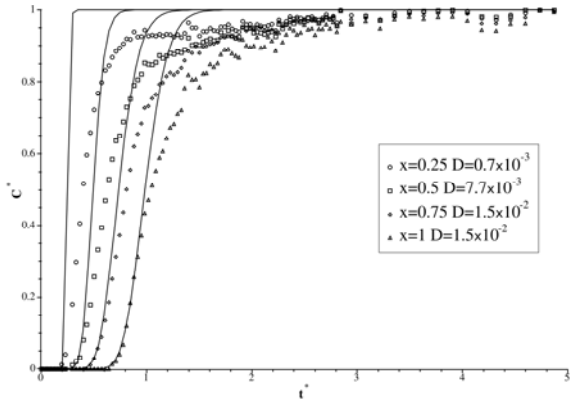

Figure 6: Concentration versus time at four different positions: $C^*=C/C0$ and $t^*=tQ/V$; scatters are experimental data sets; lines are the fits using equation (5).

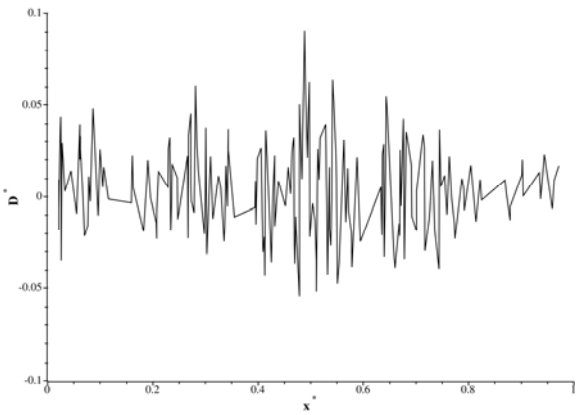

Figure 7: Determination of the dispersion coefficient on each slice: coefficient of dispersion versus position.

A piston-like flow gives a step front at each position. In a homogeneous medium with our injection conditions the concentration profiles are given by equation (5). The differences are discussed in the following section where we try to interpret the experiment with two models.

DISCUSSION

The Convection-Diffusion Approach

As said above, the common approach to analyze dispersion experiments is through the convection-diffusion equation (Equation (3)). We first tried to determine the dispersion coefficient by fitting the analytical solution (5) to the concentration profiles.
As shown in Figure (6), the results are fairly poor, especially about the second part of the curves. This may be explained by the fact that heterogeneities at the experiment scale are too important to use a homogeneous model. As a matter of fact, equation (3) assumes that properties are uniform from the inlet to position x but D may vary along the sample as any other properties like the local aperture. To take into account heterogeneities, analysis may be done at a smaller scale. The concentration is measured locally and the experimental flux F_{exp} may be derived from equation (1) Then we are able to calculate the average flux and the average concentration for each abscissa x. The dispersion coefficient may then be calculated for each position by minimizing $\left(F_{\exp}-F\right)$, with F given by equation (2). Figure (7) shows that $D^*=D\phi/\left(UL_x\right)$ fluctuates with no evident trend around an low average value, 4×10^{-3}, with a standard deviation of 15.5×10^{-3}.

Therefore, this approach is not appropriate to interpret the experiment. In particular, the convection-diffusion model has a dispersion process faster than the experiment (Figure (6)). The discrepancy may be explained by the fact that this approach takes into account molecular diffusion whereas this process should be negligible due to the high Peclet number, 5×10^3, in the experiment (Sahimi 1993)).

Capillary Model

When molecular diffusion is negligible, tracer particles are only advected. Considering laminar flow, their displacement may be described by streamtubes without solute transfer between flow paths. A very simple approach is then to model each streamtube as a capillary rectangular duct with an aperture h_i, a width δy_i and a length L_{xi}. Because of the tortuosity, L_{xi} may be greater than L_x. But considering that hi is the local hydraulic aperture characterizing each flow path, it may be assumed that tortuosity is taken into account, consequently it is assumed that $L_{xi}=L_x$. The flow is approximated by a piston-like displacement along each streamtube. The flux is then given by $F_i=U_iC_i$ and the mass balance equation (1) is:

$$\frac{\partial C_i}{\partial t}+U_i\frac{\partial C_i}{\partial x}=0 \qquad (11)$$

with C_i the local concentration, U_i the average velocity derived from a Poiseuille flow in a rectangular duct with the aperture considered small in comparison with the two other dimensions:

$$U_i=\frac{h_i^2}{12\mu}\frac{\Delta P}{L_x} \qquad (12)$$

where ΔP is the pressure drop along the flow direction, L_x is the fracture length and h_i is the

hydraulic aperture for a pressure gradient applied over the fracture. The velocity may be expressed as a function of the total flow rate *Q*:

$$U_i = \frac{h_i^2 Q}{H^3 L_y} \tag{13}$$

where H is the equivalent hydraulic aperture of the total fracture, L_y the fracture width. Dimensionless form of the mass balance equation is written:

$$\frac{\partial C_i^*}{\partial t^*} + \frac{h_i^2 \langle h \rangle}{H^3} \frac{\partial C_i^*}{\partial x^*} = 0 \tag{14}$$

With $t^* = Qt/V$, $x^* = x/L_x$ and $C^* = C/C_0$. V is the total void volume. Because the average aperture over the model is $\langle h \rangle = \sum L_{xi} \delta y_i h_i / (L_x L_y)$ then $V = L_x L_y \langle h \rangle$. Equation (14) gives the local concentration in a rectangular duct. The total concentration at x^* and t^* is then given by:

$$C^* = \frac{\sum C_i^* \delta y_i h_i}{\sum \delta y_i h_i} \tag{15}$$

$\delta y_i h_i / (\sum \delta y_i h_i)$ is noted $\theta(h_i)$ in the following. The analytical solution of equation (14) with a constant injection from a given time *t=0* corresponds to the Heaviside function defined as:

$$H\left(t^* - \frac{x^* H^3}{h_i^2 \langle h \rangle}\right) \begin{cases} H = 1 & \forall\, t^* \geq \dfrac{x^* H^3}{h_i^2 \langle h \rangle} \\ H = 0 & \forall\, t^* < \dfrac{x^* H^3}{h_i^2 \langle h \rangle} \end{cases} \tag{16}$$

Then the concentration is simply:

$$c^*(x^*, t^*) = \sum_{i=1}^{i=\tau} \theta(h_i) \quad \text{with} \quad h_\tau^2 = \frac{x^* H^3}{t^* \langle h \rangle} \tag{17}$$

The apertures map is a matrix of n_x rows (transverse direction) and n_y columns. As a first approach the fracture was divided into n_y channels of one pixel width. Each channel being a series of n_x segments with different apertures d_j, its equivalent aperture may be approximated as $h_i^3 = \langle 1/d^3 \rangle^{-1}$ (Bear 1993). The results obtained with this distribution of channels were not satisfactory: the beginning of the breakthrough curve was too fast and the end too slow. This poor result could have been expected because the ducts width used to model the streamtube distribution were too small. It was then impossible to take into account the flow complexity (tortuosity, etc.) through the equivalent aperture. In addition channels containing very small apertures will have an underestimated hydraulic aperture.

A way to reduce effects of very small apertures is to extract from this distribution a histogram with a number of bins smaller than n_y. Figure (8) shows the histogram extracted from the distribution of h_i^3 with bins size of 1/10. Their quantity is noted δy on the ordinate axis because it simply corresponds to the ducts width in dimensionless form.

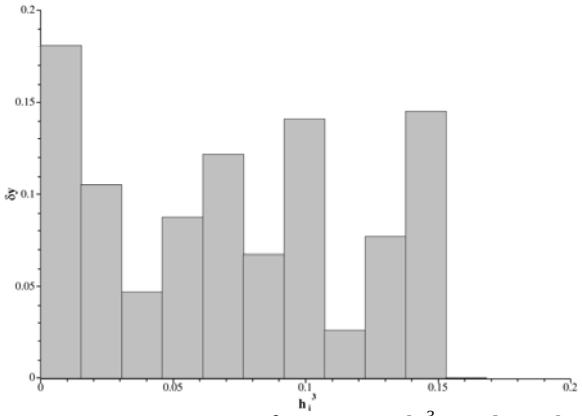

Figure 8: Histogram of apertures hi³ used in the capillary model, dy corresponds to the channels width.

Results are shown on Figure (9) for three different abscissas. For each coordinate *x* the histogram used in the analytical model is extracted from the fracture cropped from 0 to *x*. A very good agreement is observed for the outlet *x*=1, but the two others profiles show poor results. This could be easily explained by the basics of the model. One of the main assumption is that a constant pressure drop is apply over all channels between the inlet and the outlet. However the pressure map obtained by simulation (Figure (10)) clearly shows that this condition is not satisfied inside the fracture.

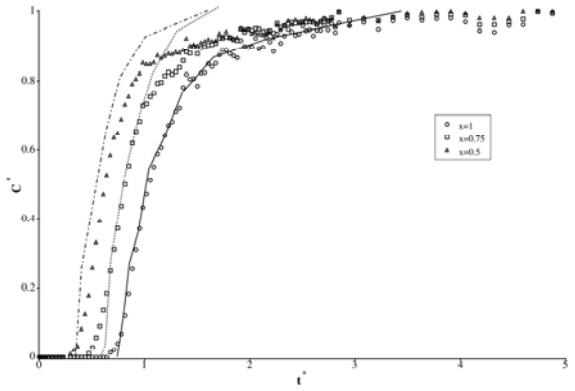

Figure 9: Concentration versus time at three abscissas: Capillary model (lines) and experiment (scatters).

This model describes the breakthrough curve using pure advection assumption. The mass flux in each

channel is not controlled either by molecular diffusion or any concentration gradient.

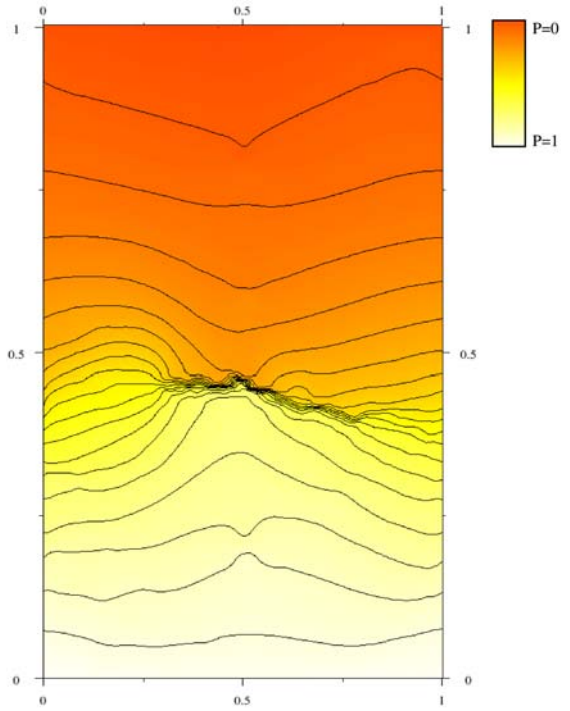

Figure 10: Numerical calculation of the pressure field using equation (10) for an incompressible fluid.

CONCLUSION

A tracer flow experiment has been performed on a resin replica of a real fracture. The set up transparency allowed flow visualization, apertures map determination, local concentration and flux calculation using the Beer-Lambert law. The estimated Peclet number was at least 5×10^3. The experiment was first interpreted using the classical convection-diffusion approach. An analytical solution for homogeneous medium has been compared to experimental concentration profiles versus time. Results were very poor. The analytical solution did not catch at all the profiles for I > 0.5 increasing faster than experimental data sets. The solution assumes that the medium was homogeneous, whereas the fracture exhibits strong heterogeneities. The local dispersion coefficient was then calculated by minimizing $F_{\exp} - F$, with F_{exp} the experimental local flux and F the theoretical flux given by the convection-diffusion approach (equation (2)). The results did not show any trend. The classical convection-diffusion approach failed to describe our tracer flow experiment. In this approach, the process catalyst is the concentration gradient, as in Fickian diffusion, whereas the high Peclet number indicates that molecular diffusion is negligible. Finally the experiment was described using a pure advective model. Assuming negligible molecular diffusion and laminar steady state flow, the fluid particles are advected along constant streamtubes. In the model, the flow paths are represented by parallel channels with hydraulic apertures taking into account tortuosity, and a piston-like flow is assumed. By calculating the channel apertures distribution from the experimental map, we were able to model the breakthrough curve. These results indicate that the approach based on pure advective description, with the dispersion process controlled by heterogeneities, gives good results.

REFERENCES

Bear, J. (1988), *Dynamics of Fluid in Porous Media*, Dover, New York.

Bear, J. (1993), *Flow and contaminant transport in fractured rock*, chap. 1. Modeling Flow and Contaminant Transport in Fractured Rocks, Bear, J. and Tsang, C.F. and de Marsily, G. ed., Academic Press, Inc., San Diego.

Bodin, J., F. Delay, and de Marsily G. (2003a), Solute transport in a single fracture with negligible matrix permeability: 1, fundamental mechanisms, *Hydrogeology Journal*, *11*, 434-454.

Bodin, J., F. Delay, and de Marsily G. (2003b), Solute transport in a single fracture with negligible matrix permeability: 2, mathematical formalism, *Hydrogeology Journal*, *11*, 434-454.

Brenner, H., and D. A. Edwards (1993), *Macrotransport processes*, Butterworth-Heinemann.
Brown, S., A. Caprihan, and R. Hardy (1998), Experimental observation of fluid flow channels in a single fracture, *Journal of Geophysical Research*, *103*(B3), 5125-5132.

Brown, S., Caprihan, A., Hardy, R., (1998), Experimental observation of fluid flow channels in a single fracture, *Journal of Geophysical Research 103(B3)*, 5125-5132.

Cussler, E. L. (1984), *Diffusion: Mass Transfer in Fluid Systems*, Cambridge University Press.

Detwiler, R. L., S. E. Pringle, and R. J. Glass (1999), Measurement of fracture aperture felds using transmitted light: An evaluation of measurement errors and their influence on simulations of flow and transport through a single fracture, *Water Resources Research*, *35*(9), 2605-2617.

Detwiler, R. L., H. Surname, and R. Surname (2000), Solute transport in variable-aperture fractures: an investigation of the relative importance of taylor

dispersion and macrodispersion, *Water Resources Research*, *36*(7), 1611-1625.

Dullien, F. (1992), *Porous Media: Fluid Transport and Pore Structure*, 2nd ed., Academic Press, San Diego.

Dutta, D., and D. T. Leighton (2001), Dispersion reduction in pressure-driven flow through microetched channels, *Analalytical Chemistry*, *73*(3), 504 - 513.

Forchheimer, P. (1914), *Hydraulik*, Teubner, Leipzig and Berlin.

Fourar, M., S. Bories, R. Lenormand, and P. Persoff (1993), Two-phase flow in smooth and rough fractures: measurement and correlation by porous-medium and pipe flow models, *Water Resources Research*, *29*(11), 3699-3708.

Grindrod, P., and M. D. Impey (1993), Channeling and fickian dispersion in fractal simulated porous media, *Water Resources Research*, *29*(12), 4077-4089.

Harris, R. M. (1999), *Coloring Technology for Plastics*, chap. A Primer on Colorful Additives, harris, r. m. ed., William Andrew Publishing.

Isakov, E., S. Ogilvie, C. Taylor, and P. Surname (2001), Fluid flow through rough fractures in rocks i: high resolution aperture determinations, *Earth and Planetary Science Letters*, *191*, 267-282.

Lee, J., J. M. Kang, and J. Choe (2003), Experimental analysis on the effects of variable apertures on tracer transport, *Water Resources Research*, *39*(1), 1015-1025.

Neretnieks, I. (2002), A stochastic multi-channel model for solute transportâ€"analysis of tracer tests in fractured rock, *Journal of Contaminant Hydrology*, *55*, 175-211.

Persoff, P., and K. Pruess (1995), Two-phase flow visualization and relative permeability measurement in natural rough-walled rock fractures, *Water Resources Research*, *31*(5), 1175-1186.

Renard, P., and G. de Marsily (1997), Calculating equivalent permeability: A review, *Advances in Water Resources*, *20*(5-6), 253-278.

Sahimi, M. (1993), Flow phenomena in rocks: from continuum models to fractals, percolation, cellular automata, and simulated annealing, *Reviews of Modern Physics*, *62*(4), 1393-1534.

Zimmermann, R., and I. Main (2004), *Mechanics of Fluid-Saturated Rocks*, chap. Hydromechanical Behaviour of Fractured Rocks, pp. 363-422, Elsevier Academic Press.